

Article

Inverse Evaluation of Monopile Pile–Soil Interaction Parameters Using Random Search

Hou Qiao ^{1,2} , Wei Li ¹, Zhenqiang Jiang ¹, Xi Sheng ² and Chuanrui Guo ^{2,*} 

¹ Key Laboratory of Far-shore Wind Power Technology of Zhejiang Province, POWERCHINA HUADONG Engineering Corporation Limited (HDEC), Hangzhou 311122, China; qiaohou@gmail.com (H.Q.); li_w@hdec.com (W.L.); jiang_zq@hdec.com (Z.J.)

² Institute of Urban Smart Transportation & Safety Maintenance, College of Civil and Transportation Engineering, Shenzhen University, Shenzhen 518061, China; shengxi1107@163.com

* Correspondence: cguo@szu.edu.cn

Abstract: To deal with the uncertainties in modeling offshore wind turbines, we propose a parameter inversion method for the pile–soil interaction model based on structural health monitoring results and the numerical model. The proposed parameter inversion method has a numerical model, an objective function selected using both the numerical and identified results, and an inverse optimization using a random search algorithm in the assumed parameter space. The parameter results in the minimum optimization objective function are identified as the in situ parameter. The proposed method is confirmed to converge after some number of iterations, depending on what the initial parameter values are. However, different initial parameter cases may converge to slightly different optimal parameters, implying that the pile results are sensitive to geological parameters. Moreover, a comparison with the original design results shows design redundancy or risks. Though the proposed method has several flaws, it can shed light on the influence of parameter uncertainties on offshore wind turbines.

Keywords: offshore wind; parameter inversion; pile–soil interaction; random search



Citation: Hou, Q.; Wei, L.; Zhenqiang, J.; Xi, S.; Chuanrui, G. Inverse Evaluation of Monopile Pile–Soil Interaction Parameters Using Random Search. *J. Mar. Sci. Eng.* **2023**, *11*, 1329. <https://doi.org/10.3390/jmse11071329>

Academic Editor: Dong-Sheng Jeng

Received: 7 June 2023

Revised: 23 June 2023

Accepted: 26 June 2023

Published: 29 June 2023



Copyright: © 2023 by the authors. Licensee MDPI, Basel, Switzerland. This article is an open access article distributed under the terms and conditions of the Creative Commons Attribution (CC BY) license (<https://creativecommons.org/licenses/by/4.0/>).

1. Introduction

Currently, most offshore wind farms have structural health monitoring systems that record extensive in situ operation data at a predefined time resolution. However, during monitoring, these operation data are often mixed with signal disturbances in the ocean environment. Furthermore, a large portion of monitoring data is usually archived as mean, median, or maximum values over a certain period to reduce data storage. Therefore, it is very challenging to analyze the monitoring data, neither identifying nor predicting possible faults in offshore wind turbines.

Nonetheless, plenty of exciting work has been conducted worldwide on structural health monitoring data analysis. Jahani [1] discussed the crucial concerns related to the structural dynamics of offshore wind turbines. The resonance frequencies and damping values of dominant mode shapes for a parked wind turbine are tracked using an automated state-of-the-art operational modal analysis technique [2]. Modal parameters were used as a baseline for long-term observations [3]. Estimates of natural frequencies, damping ratios, and mode shapes of offshore wind turbines were obtained by the poly-reference least squares complex frequency-domain estimator (PolyMAX) and the covariance-driven stochastic subspace identification (SSI-COV) method [4]. The stochastic subspace identification method has been used to reveal the modal parameters of offshore wind turbines experiencing earthquakes [5]. Substructure damping [6], aerodynamic damping [7], and damping of wind turbine towers [8] have all been discussed, and Eigensystem Realization Algorithm (ERA), SSI-COV, the Enhanced Frequency Domain Decomposition (EFDD) [8], and

time-frequency analysis [7] have all been used. Estimating offshore wind turbine damping using state-of-the-art operational modal analysis (OMA) techniques was summarized in [9]. Besides, the relationship between modal parameters and environmental/operational factors was illustrated [10], and vibration-based damage detection was also discussed [11].

Meanwhile, analyzing and utilizing offshore wind turbine monitoring data is challenging, as the marine environment is full of interference signals. To reduce the adverse effects of interference, Dong [12] proposed a modified stochastic subspace identification (SSI) method considering known and time-invariant harmonic interference. A time-frequency method based on single-mode function (SMF) decomposition was presented to reduce mode mixing and data contamination effects in [13]. Data containing high-energy components were identified by adopting iterative noise elimination by Liu [14], which was confirmed to be better than the stochastic subspace identification method. Noise cleansing and missing data imputation were found to increase the accuracy of fatigue assessment when mutually applied [15]. Multi-dimensional information fusion was used based on Dempster-Shafer (D-S) evidence theory for the fault diagnosis of wind turbines in [16]. In this paper, the monitoring data was confirmed to be mixed with trend terms in polynomial form. Therefore, the noise can be removed by a preprocessing algorithm for removing trend items; the details are not provided here, as they are common practice.

Offshore wind turbines are seldom equipped with environmental monitoring or load monitoring equipment. Therefore, the response of offshore wind turbines is always an output-only identification problem, with these related excitations being absent [17–19]. In the meantime, as offshore wind turbines are always modeled using a linear beam and the soil-structure interaction is considered using American Petroleum Institute (API) based reaction springs attached to the monopile [20], the uncertainty in soil modeling is always overlooked [21–24]. Andersen [21] studied the first natural frequency of a monopile foundation interacting with clay-type soil having a spatial variation of properties. They found that if the undrained shear strength of the soil has a log-normal distribution, the probability density functions (PDFs) for the pilehead stiffness components are also log-normal as well. However, this is different for the natural frequency. Damgaard [25] found that soil-structure interaction is critical in offshore wind turbine design. Therefore, it is possible to obtain good dynamic modeling of offshore wind turbines only after tuning the first natural frequency and damping. Arany [26] found that the cross-coupling spring term needs to be included in the offshore wind foundation analysis. Zania [27] found that soil properties mainly affected the modified soil-structure interaction eigenfrequency and damping of slender engineering structures, such as offshore wind turbines. The dynamic soil-structure interaction may drive even a conservative design to restrictive frequency ranges. Many more results show that the dynamic response of a wind turbine is highly sensitive to the properties of the soil where it has been built [22–24]. To deal with the uncertainty in the modeling and excitation of offshore wind turbines, we propose an inverse evaluation method that can fit the numerical model to the in situ monitoring data using the parameters identified here, which can be considered the in situ parameters.

The motivation of this paper is to propose a method to identify the in situ parameters of offshore wind turbines and analyze the influence of uncertainty on the initial design parameters. In Section 2, the methods related to the inverse evaluation are provided. The results obtained from the inverse evaluation method are discussed in Section 3. Subsequently, Section 4 ends with conclusions.

2. Methods for Inverse Evaluation

In this section, we first briefly introduce the sensor deployment and the monitoring data. Then, the data are analyzed using different operational modal analysis methods. The results of the operational modal analysis are analyzed to check whether there are invariant (stable) modal frequencies during a relatively long time. After the invariant modal frequencies are obtained, they can be used to construct the inverse optimization

objective function. Subsequently, the pile–soil interaction parameters of the monopile can be identified using the optimization objective function.

2.1. Monitoring Data and Sensors

The monitoring data was obtained from a monopile in an offshore wind farm in the eastern China Sea, where the water depth is about 10 m. The monopile foundation was installed with a 4.5 MW offshore wind turbine. The total length of the pile foundation is 54 m, the axial compression capacity is 27,887 kN, and the allowable frequency range for the wind turbine design is 0.24 to 0.32 Hz. The configuration of acceleration sensors on the wind turbine is shown in Figure 1. These accelerations are used in the following analysis.

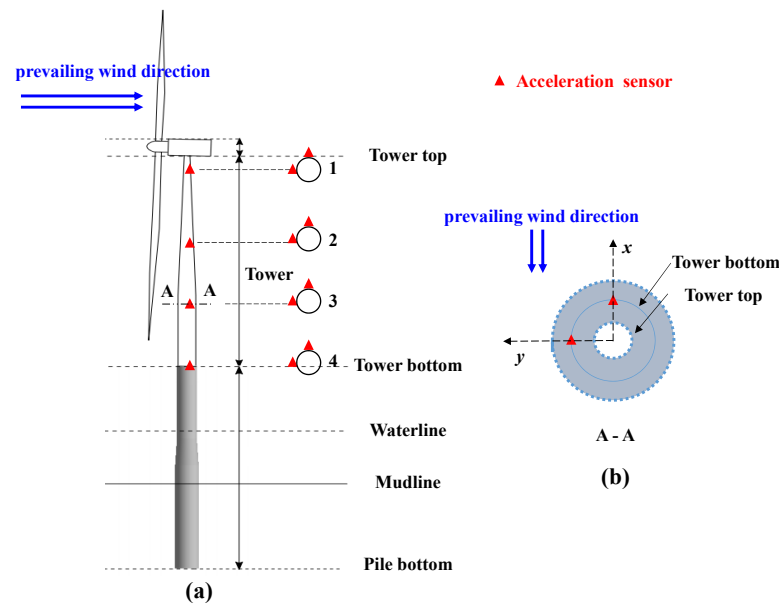


Figure 1. Acceleration sensors on the tower: (a) front view and (b) top view of section A-A.

The monitoring data consisted of accelerations from four elevations on the wind turbine tower within 24 h. The data were stored in 24 files (sampling time of about 60 min each), with a sampling frequency $F_s = 50$ Hz. During the monitoring period, the rotation speed of the wind turbine was 3.20 to 10.57 revolutions per minute (rpm). The monitoring points are listed in Table 1.

Table 1. Acceleration monitoring points (elevation: m, acceleration: m/s^2).

Location	Sensor ID	Elevation	Direction ¹
1	J1	88 m	X
1	J2	88 m	Y
2	J3	60 m	X
2	J4	60 m	Y
3	J5	32 m	X
3	J6	32 m	Y
4	J7	12 m	X
4	J8	12 m	Y

¹ X-direction: prevailing wind direction; Y-direction: vertical to prevailing wind direction.

From this wind farm, we obtained the prevailing wind direction according to the wind data observed over two years, using the definition that the direction with the longest accumulated occurrence time in a year or the direction with the longest petals in the annual wind rose-petal chart developed by the local meteorological department. Meanwhile, according to the official documentation of the offshore wind farm we investigated, no pile

slope was recorded during pile driving, and the wind farm is not located in seismically active areas. Therefore, pile slope and soil liquefaction during pile driving is not considered.

2.2. Analysis of In Situ Modal Frequency Characteristics

This section uses operational modal analysis methods to analyze the monitoring data. However, the modal characteristics should be confirmed as stable before conducting the inverse evaluation of the monopile. Subsequently, inverse evaluation can be performed as follows: based on the stable modal characteristics, an objective function for parameter optimization is constructed, then an optimization algorithm is used for the inverse analysis of the in situ parameters.

Modal Identification Based on Subspace Identification

The stochastic subspace identification (SSI) method is a dynamic identification method that can deal with dynamic systems with uncertain inputs. This method constructs the Hankel matrix using the existing data, then forms the Toeplitz matrix to solve the coefficient matrices (SSI-COV, covariance-driven stochastic subspace identification) or forms the output projection matrix to solve the coefficient matrices (SSI-DATA, data-driven stochastic subspace identification). The SSI-COV algorithm is shown in the following steps. Assuming that there are l measuring points (possibly different sensor types), the following Hankel matrix is constructed by selecting r points as reference data [28]:

$$\mathbf{H} = \frac{1}{\sqrt{s}} \begin{pmatrix} \mathbf{y}_0^{\text{ref}} & \mathbf{y}_1^{\text{ref}} & \cdots & \mathbf{y}_{s-1}^{\text{ref}} \\ \mathbf{y}_1^{\text{ref}} & \mathbf{y}_2^{\text{ref}} & \cdots & \mathbf{y}_s^{\text{ref}} \\ \cdots & \cdots & \cdots & \cdots \\ \mathbf{y}_{i-1}^{\text{ref}} & \mathbf{y}_i^{\text{ref}} & \cdots & \mathbf{y}_{i+s-2}^{\text{ref}} \\ \mathbf{y}_i & \mathbf{y}_{i+1} & \cdots & \mathbf{y}_{i+s-1} \\ \mathbf{y}_{i+1} & \mathbf{y}_{i+2} & \cdots & \mathbf{y}_{i+s} \\ \cdots & \cdots & \cdots & \cdots \\ \mathbf{y}_{2i-1} & \mathbf{y}_{2i} & \cdots & \mathbf{y}_{2i+s-2} \end{pmatrix} = \begin{pmatrix} \mathbf{Y}_{0|i-1}^{\text{ref}} \\ \mathbf{Y}_{i|2i-1}^{\text{ref}} \end{pmatrix} = \begin{pmatrix} \mathbf{Y}_p^{\text{ref}} \\ \mathbf{Y}_f \end{pmatrix} \begin{matrix} \updownarrow ri \times s \\ \updownarrow li \times s \end{matrix} \quad (1)$$

where $\mathbf{y}_0^{\text{ref}} \sim \mathbf{y}_{i+s-2}^{\text{ref}}$ and $\mathbf{y}_i \sim \mathbf{y}_{2i+s-2}$ are column vectors composed of r reference data and l measuring data, respectively, and s is the order of the model. Assuming that the dynamic system is ergodic, the block Toeplitz matrix $\mathbf{T}_{1|i}^{\text{ref}}$ is composed of the covariance between the measurement data and the reference data, which satisfies

$$\mathbf{T}_{1|i}^{\text{ref}} = \mathbf{y}_f \left(\mathbf{y}_p^{\text{ref}} \right)^T \quad (2)$$

The block Toeplitz matrix $\mathbf{T}_{1|i}^{\text{ref}}$ can be decomposed into [28]

$$\mathbf{T}_{1|i}^{\text{ref}} = \begin{pmatrix} \mathbf{C} \\ \mathbf{CA} \\ \vdots \\ \mathbf{CA}^{i-1} \end{pmatrix} \begin{pmatrix} \mathbf{A}^{i-1} \mathbf{G}^{\text{ref}} & \mathbf{A}^{i-2} \mathbf{G}^{\text{ref}} & \cdots & \mathbf{A} \mathbf{G}^{\text{ref}} \mathbf{G}^{\text{ref}} \end{pmatrix} = \mathbf{O}_i \mathbf{C}_i^{\text{ref}} \quad (3)$$

where

$$\mathbf{G}^{\text{ref}} = E \left[\mathbf{x}(k+1) \left(\mathbf{y}_p^{\text{ref}} \right)^T \right]$$

is the covariance of the state data and reference output data.

After the block Toeplitz matrix $\mathbf{T}_{1|i}^{\text{ref}}$ is obtained from Equations (1) and (2), the observability matrix and controllability matrix, i.e., \mathbf{O}_i and \mathbf{C}_i in Equation (3), can be solved by singular value decomposition (SVD) of $\mathbf{T}_{1|i}^{\text{ref}}$. Subsequently, the state matrices (\mathbf{A} and \mathbf{C})

of the dynamic system can be obtained. The modal characteristics are the eigenvalues (eigenvectors) of the state matrices [28,29]:

$$\Psi = \Psi_A, \quad \lambda = \frac{\ln(\lambda_A)}{\Delta t}, \quad f = \frac{|\lambda|}{2\pi}, \quad \zeta = -\frac{\text{Re}(\lambda)}{|\lambda|} \tag{4}$$

where Ψ_A and λ_A are the eigenvectors and eigenvalues, respectively, of the state space matrix and Ψ , λ , f , and ζ are the system’s mode shape, complex eigenvalue, natural frequency, and damping ratio.

Another modal identification method originating from control theory is the subspace identification method, which includes several variants, including N4SID (numerical algorithms for subspace state space system identification), MOESP (multivariable output error state space), and CVA (canonical variable analysis) [30]. As the three subspace algorithms are special cases, with each of the algorithms a specific choice of the weighting matrices [30], only N4SID is selected as a concept demonstration example, shown below.

The N4SID algorithm begins with the discrete-form equation of a dynamic system [31,32]

$$\mathbf{x}_{k+1} = \mathbf{A}\mathbf{x}_k + \mathbf{B}\mathbf{u}_k + \mathbf{w}_k, \quad \mathbf{y}_k = \mathbf{C}\mathbf{x}_k + \mathbf{D}\mathbf{u}_k + \mathbf{v}_k \tag{5}$$

where \mathbf{A} , \mathbf{B} , \mathbf{C} , and \mathbf{D} are the coefficient matrices of the state space, \mathbf{u}_k , \mathbf{y}_k , and \mathbf{x}_k are the input vectors, output vectors, and state vectors, respectively, and \mathbf{w}_k and \mathbf{v}_k are the state noise and measurement noise vectors, respectively. Based on Equation (5), we can obtain

$$\begin{aligned} \begin{bmatrix} \mathbf{y}_k \\ \mathbf{y}_{k+1} \\ \vdots \\ \mathbf{y}_{k+s-1} \end{bmatrix} &= \underbrace{\begin{bmatrix} \mathbf{C} \\ \mathbf{CA} \\ \vdots \\ \mathbf{CA}^{s-1} \end{bmatrix}}_{\mathbf{I}_s} \mathbf{x}_k + \underbrace{\begin{bmatrix} \mathbf{D} & & & \\ \mathbf{CB} & \mathbf{D} & & \\ \vdots & \vdots & \ddots & \\ \mathbf{CA}^{s-2}\mathbf{B} & \dots & \mathbf{CB} & \mathbf{D} \end{bmatrix}}_{\mathbf{H}_s} \begin{bmatrix} \mathbf{u}_k \\ \mathbf{u}_{k+1} \\ \vdots \\ \mathbf{u}_{k+s-1} \end{bmatrix} + \\ &\underbrace{\begin{bmatrix} 0 & & & \\ \mathbf{C} & 0 & & \\ \vdots & \vdots & \ddots & \\ \mathbf{CA}^{s-2} & \dots & \mathbf{C} & 0 \end{bmatrix}}_{\mathbf{G}_s} \begin{bmatrix} \mathbf{w}_k \\ \mathbf{w}_{k+1} \\ \vdots \\ \mathbf{w}_{k+s-1} \end{bmatrix} + \underbrace{\begin{bmatrix} 1 & & & \\ 0 & 1 & & \\ \vdots & \vdots & \ddots & \\ 0 & \dots & 0 & 1 \end{bmatrix}}_{\mathbf{I}_s} \begin{bmatrix} \mathbf{v}_k \\ \mathbf{v}_{k+1} \\ \vdots \\ \mathbf{v}_{k+s-1} \end{bmatrix} \end{aligned}$$

The model order s should be larger than the system order.

$$s \geq \max\{\text{Rand}(\mathbf{A}), \text{Rand}(\mathbf{B}), \text{Rand}(\mathbf{C})\}.$$

Let

$$\mathbf{X}_N = [\mathbf{x}_1 \quad \mathbf{x}_2 \quad \dots \quad \mathbf{x}_N]_{1 \times N} \tag{6}$$

$$\mathbf{Y}_{sN} = \begin{bmatrix} \mathbf{y}_1 & \mathbf{y}_2 & \dots & \mathbf{y}_N \\ \mathbf{y}_2 & \mathbf{y}_3 & \dots & \mathbf{y}_{N+1} \\ \vdots & \vdots & \ddots & \vdots \\ \mathbf{y}_s & \mathbf{y}_{s+1} & \dots & \mathbf{y}_{s+N-1} \end{bmatrix}_{s \times N}, \quad \mathbf{U}_{sN} = \begin{bmatrix} \mathbf{u}_1 & \mathbf{u}_2 & \dots & \mathbf{u}_N \\ \mathbf{u}_2 & \mathbf{u}_3 & \dots & \mathbf{u}_{N+1} \\ \vdots & \vdots & \ddots & \vdots \\ \mathbf{u}_s & \mathbf{u}_{s+1} & \dots & \mathbf{u}_{s+N-1} \end{bmatrix}_{s \times N} \tag{7}$$

$$\mathbf{W}_{sN} = \begin{bmatrix} \mathbf{w}_1 & \mathbf{w}_2 & \dots & \mathbf{w}_N \\ \mathbf{w}_2 & \mathbf{w}_3 & \dots & \mathbf{w}_{N+1} \\ \vdots & \vdots & \ddots & \vdots \\ \mathbf{w}_s & \mathbf{w}_{s+1} & \dots & \mathbf{w}_{s+N-1} \end{bmatrix}_{s \times N}, \quad \mathbf{V}_{sN} = \begin{bmatrix} \mathbf{v}_1 & \mathbf{v}_2 & \dots & \mathbf{v}_N \\ \mathbf{v}_2 & \mathbf{v}_3 & \dots & \mathbf{v}_{N+1} \\ \vdots & \vdots & \ddots & \vdots \\ \mathbf{v}_s & \mathbf{v}_{s+1} & \dots & \mathbf{v}_{s+N-1} \end{bmatrix}_{s \times N} \tag{8}$$

$$\Gamma_s = \begin{bmatrix} C \\ CA \\ \vdots \\ CA^{s-1} \end{bmatrix}, \quad H_s = \begin{bmatrix} D & & \\ CB & D & \\ \vdots & \vdots & \ddots \\ CA^{s-2}B & \dots & CB & D \end{bmatrix} \tag{9}$$

$$G_s = \begin{bmatrix} 0 & & & \\ C & 0 & & \\ \vdots & \vdots & \ddots & \\ CA^{s-2} & \dots & C & 0 \end{bmatrix}, \quad I_s = \begin{bmatrix} 1 & & & \\ 0 & 1 & & \\ \vdots & \vdots & \ddots & \\ 0 & \dots & 0 & 1 \end{bmatrix} \tag{10}$$

According to the above definition, the extended system equation is

$$Y_{sN} = \Gamma_s X_N + H_s U_{sN} + G_s W_{sN} + I_s V_{sN}. \tag{11}$$

Assuming that the system states are ergodic and the system input is independent of the state and measurement noise, the matrices Γ_s , H_s , and G_s can then be obtained by the convex optimization least squares method using Equation (11). Subsequently, the state matrices A , B , C , and D of the dynamic system in Equation (5) can be obtained using the block matrix projection relationship in Equations (6)–(10). The modal characteristics represent the eigenvalues (eigenvectors) of the state matrices.

To perform an inverse evaluation based on dynamic characteristics, it is necessary to check whether the modal characteristics are stable. The objective function of the inverse optimization can only be constructed based on these stable modal characteristics. Subsequently, inverse evaluation can be performed using an optimization algorithm according to the pre-mentioned inverse optimization function.

2.3. Methods for Inverse Evaluation

When offshore wind turbines are installed, their in situ working state can only be tracked by structural health monitoring systems. However, structural monitoring systems are rarely equipped with environmental monitoring devices, which are always extremely expensive. Therefore, it is not easy to numerically evaluate the in situ response of offshore wind turbines as the input (excitation load and environment data) and output (response) cannot be obtained simultaneously. To evaluate the in situ state of offshore wind turbines, we propose an inverse evaluation method based on modal characteristics. The implementation procedures are provided below.

2.3.1. Physical Model for Inverse Evaluation

A numerical model of the monopile should be established to perform the inverse evaluation procedure as a prerequisite of the optimization step.

For offshore wind turbines, as the main structural components such as the turbine foundation, tower, or blades are always long and slender, these structural components are always considered as beams or bars. In contrast, flanges and other local masses are modeled as concentrated mass points.

Monopiles with different marine soils are permanently installed far offshore, where wind, waves, and currents are present. According to the regular wave theory selection diagram in IEC 61400-3-1 [33] (Annex B), H/gT^2 is 0.01 and d/gT^2 is 0.019; therefore, the seventh-order stream function theory is used to model waves. The current is considered using the standard velocity profile in IEC 61400-3-1. However, the wind load is not calculated here; only the results provided by the wind turbine supplier are used.

As the physical properties of marine soil are highly dispersed [34–37], the soil–structure interaction of offshore wind turbines is one of the prominent sources of uncertainty in their dynamic response [22–24]. These uncertainties could lead to disturbances in the condition evaluation of offshore wind turbines that cannot be ignored. Currently, soil reaction curves for piles under axial compression or lateral loads, i.e., $t - z$, $Q - z$ and

$p - y$ in American Petroleum Institute (API) RP 2GEO [37] (or their recently-developed modified variants, such as the PISA model [38]) and classical soil constitutive models included in commercial finite element software are commonly used. As the soil reaction curves are easy to implement and have lower computational costs, they are used to show the proposed methodology.

To reduce the modeling uncertainty of offshore wind turbines, the inverse evaluation method is based on in situ optimization of the soil–structure interaction parameters, which are one of the primary sources of uncertainties in offshore wind turbine modeling and analysis. Recently, it has been argued that the soil reaction curves can be rather conservative with regard to the soil response [38]. However, the proposed method may be enlightening, even though the parameters may suffer from a deficiency in model assumptions.

A schematic of the physical model proposed for offshore wind turbines is shown in Figure 2.

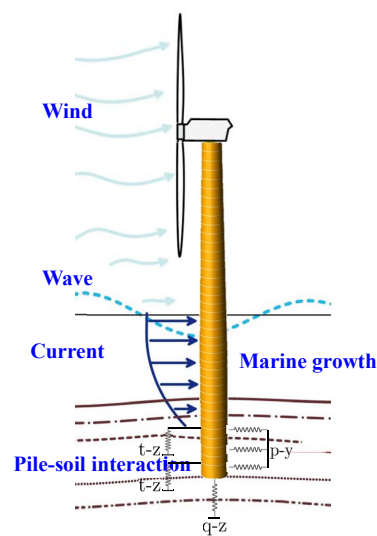


Figure 2. Physical model of offshore wind turbine.

In the numerical model, the structural geometry, materials, site conditions, and loads of the offshore wind turbines are first provided in several input files. A series of soil springs are formed to simulate the soil reaction response, and a required amount of wind, wave, current, and other external conditions are combined to obtain the environmental boundary conditions. Then, a collection of solution programs operate on these inputs, producing a solution containing joint displacements and internal element forces. Subsequently, another category of postprocessing programs evaluates the structure response using the solution shown above.

2.3.2. Objective Function for Inverse Evaluation

This paper combines the in situ modal identification results using structural monitoring data and numerical results obtained to form the objective function. In order to accomplish this, it should first be confirmed that the modal identification results are stable over a relatively long time, such as one day (twenty-four hours). Otherwise, the objective function based on the obtained results does not make sense, as it varies without parameter variations.

The objective function is selected as follows:

$$G(f_{\text{num}}, \hat{f}, \alpha) = \left\| f_{\text{num}} - \hat{f}_{-1-\alpha}^{1+\alpha} \right\| \tag{12}$$

where $\|\cdot\|$ denotes the 2-norm, f_{num} and \hat{f} are the first-order modal frequency obtained by the numerical model and that obtained by the monitored data, respectively, and $f_{1-\alpha}^{1+\alpha}$ represents the first-order modal results that match f_{num} , defined as the minimum \hat{f} value satisfying

$$\hat{f}(1 - \alpha) \leq f_{\text{num}} \leq \hat{f}(1 + \alpha), \tag{13}$$

where α is the variation ratio of the modal frequencies, which measures the span where the modal frequency varies, $\alpha = 0.05 \sim 0.1$ (DNV-ST-0126 [39]).

After the objective function is defined, to find the optimal value that best fits the in situ data, the inverse evaluation procedure should traverse as many values in the parameter space as possible, if not all.

2.3.3. Parameter Space for Inverse Evaluation

According to the geotechnical report of the wind farm, the investigated offshore wind turbine is installed on a site with eight strata of marine soil, with 42 total parameters comprising nine different types. The soil–structure interaction parameters are provided in Table 2.

Table 2. Pile–soil interaction parameters for offshore wind turbine (API).

Parameters		Units
	Effective weight γ'	kN/m ³
Sand	Internal friction angle ϕ	Degree
	Relative density D_r	/
	Pile-soil friction angle δ	Degree
	Ultimate value of pile side friction resistance f_{max}	kPa
	Bearing capacity factor N_q	/
	Ultimate axial capacities of unit pile end p_{max}	kPa
Clay	Undrained shear strength C_u	kPa
	ϵ_{50}	/

The statistical distribution of the soil parameters is highly spatially discrete. Therefore, the variation of the soil parameters can be assumed to follow a normal or log-normal distribution [34,35]. It is assumed that the parameter X of the soil–structure interaction model in different soil layers obeys the normal distribution, with a mean value μ provided by the geological survey (the value X_0 used for foundation design), $\mu = X_0$, and coefficient of variation κ between 0 and 0.5, $\kappa = 0 \sim 0.5$, that is,

$$X \sim N(X_0, \sigma_X^2) \tag{14}$$

where $\sigma_X = \kappa X_0$. The coefficient of variation is not the same for all parameters in reality. However, without loss of generality, an identical and constant coefficient of variation κ is used here to conduct a proof of concept for the inverse evaluation method.

It is assumed that the parameters in different strata are independent and that only related parameters are considered in a single soil stratum, depending on the soil classification. In the sensitivity analysis, all parameters are kept constant in every other stratum. Meanwhile, relations between different parameters in a given stratum are employed to reduce the number of independent parameters per stratum.

After considering all of the above constraints, a screening process is first conducted to select parameters with higher single-factor sensitivity through sensitivity analysis to reduce the number of parameters for inverse optimization. Then, the chosen parameters are assumed to follow the distribution defined in Equation (14), and three to five representative values are randomly selected as the inputs for the optimization algorithm at each iteration.

2.3.4. Random Search Algorithm for Inverse Evaluation

Global optimization methods include grid search, random search, Bayesian optimization, gradient-based optimization, etc. As the efficiency of grid search is limited by the number of parameters and the values of parameters, Bayesian optimization relies on prior information to establish the probability model of the search parameters and objective function, and gradient-based optimization can quickly run into local optimization situations, a random optimization algorithm is used here for global optimization of the pile–soil interaction parameters. Moreover, the random optimization algorithm is a good choice, as there are many soil parameters for which the distribution is roughly unknown, and this algorithm can obtain globally optimized results in fewer iterations than grid search [40].

Considering the upper and lower bounds of the parameters, the random search algorithm takes a random combination of parameter values from the interval and carries out parameter updating through an iterative process. In addition, by designing a suitable parameter updating algorithm, random search can overcome the limitations caused by assumptions about the initial parameter distribution.

The random search algorithm can be implemented using the following steps:

1. Define the objective function $G(X)$, penalty function $P(f, \alpha)$, and coefficient α (if used). The convergence criteria and the maximum number of iterations should be set as well.
2. Determine the upper and lower bounds of the parameters $[X]$ and estimate the distribution $X \sim f_X(x)$.
3. Set an initial parameter value X_0 and solve the initial objective function value $G(X_0)$.
4. Generate m random parameter values $\hat{X}_1, \hat{X}_2, \dots, \hat{X}_m$ according to parameter distribution $f_X(x)$ and solve $G(\hat{X}_i)$, where $i = 1, 2, \dots, m$. If $\min[G(\hat{X}_i)] > G(X_0)$, repeat Step 4 until $\min[G(\hat{X}_i)] \leq G(X_0)$.
5. If there exists $\min[G(\hat{X}_i)] \leq G(X_0)$, set $X_0 = \hat{X}_i$. Repeat Steps 3 and 4 until the iteration reaches the convergence criteria or the maximum number of iterations. The final \hat{X}_i is the optimized parameter value under the convergence criteria or the maximum number of iterations.

The flow chart of the random search algorithm is shown in Figure 3.

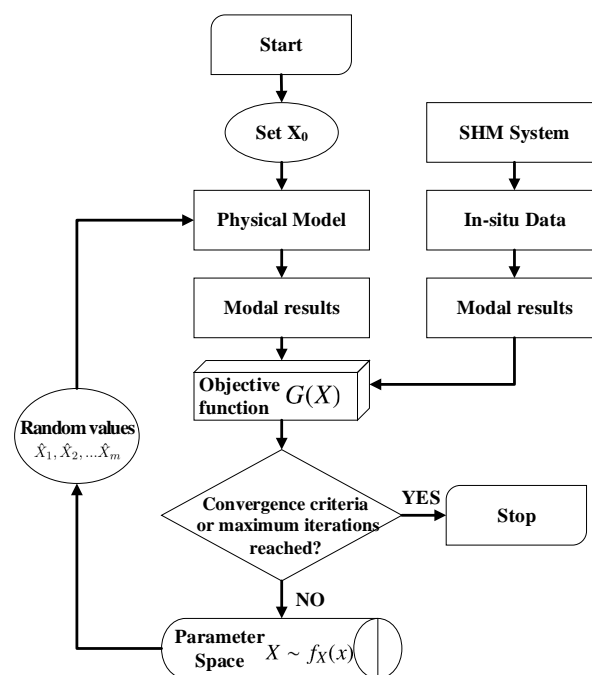


Figure 3. Flow chart of the random search algorithm

After the in situ modal frequencies of monopiles are identified as stable, an objective function can be selected using both the numerical and modal identification results.

Subsequently, inverse optimization can be performed using a random search algorithm in the assumed parameter space. The parameter results in the minimum optimization objective function are identified as the in situ parameter of the monopile, as this results in the numerical model best approximating the in situ structure.

3. Results and Discussion

To analyze the in situ state of offshore wind turbines, inverse evaluation is performed here to obtain their in situ parameters based on a random search algorithm using numerical modal results and those identified from monitored data. The parameters used in the numerical model are provided in Table 3. A scour depth of 6 m was used in the numerical model according to the site conditions and experience from offshore wind farms nearby.

Table 3. Parameters used in the numerical model.

	Value	Units	Description
Rated capacity	4.5	MW	Variable-pitch variable-speed
Drag coefficient C_d	1.2	/	Marine growth included
Inertia coefficient C_m	2.0	/	Marine growth included
Marine growth thickness	10	cm	/
50 year return wave height H_{50}	2.90	m	/
50 year return wave period T_{50}	7.06	s	/
Bottom velocity	2.310	m/s	/
Pile diameter	5.5	m	/
Mudline level	−9.5	m	/

The soil parameters from the geological survey are listed in Table 4 (not all).

Table 4. Parameters for the offshore wind turbine installation site.

Stratums	γ'	ϕ	D_r	δ	f_{max}	N_q	p_{max}	C_u	ϵ_{50}
silt	8.5	28	0.2	23	75	/	/	/	/
silt	9.3	32	0.35	27	87	/	/	/	/
silt	9.4	33	0.4	28	87	/	/	/	/
clay	9.2	/	/	/	/	/	/	60	0.008
clay	8.4	/	/	/	/	/	/	40	0.015
sand	9.6	34	0.45	29	93	36	8640	/	/
sand	9.9	35	0.5	30	96	40	9600	/	/
sand	9.9	36	0.6	31	99	42	10,080	/	/

This manuscript considers a total of eight strata, including forty-two parameters of nine different types. It is assumed that the parameters in different strata are independent, and only three to seven parameters are considered in a single soil stratum, depending on the soil classification. Therefore, in the sensitivity analysis, all parameters are kept constant in every other stratum. Meanwhile, relations between different parameters in a stratum are employed to reduce the number of independent parameters per stratum. After considering all the constraints above, a screening process is conducted to select higher-sensitivity parameters, after which the chosen parameters are assumed to follow the normal distribution, and three to five representative values are randomly chosen as the inputs for the optimization algorithm at each iteration.

3.1. Operational Modal Analysis

The operational modal results are first analyzed to check whether stable in situ modal frequencies exist, as this is a prerequisite for the inverse optimization step.

3.1.1. Verification of Stable Modes

Both SSI-COV, SSI-DATA, and N4SID are used in operational modal identification for mutual verification. In the modal identification procedures, the model order s is assumed to be 40. The modal results confirmed that the model order s is suitable (results not included here). The modal convergence criteria are set to an error in modal frequency and damping ratio no greater than one and 5%, respectively, and a mode shape consistency no less than 99%.

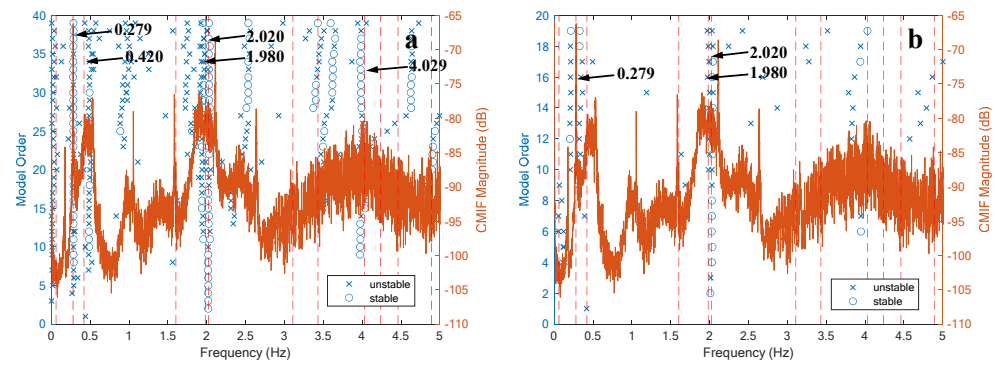


Figure 4. Results from different methods: (a) SSI-COV and (b) SSI-DATA. The vertical dashed line shows N4SID results, while \circ and \times respectively correspond to stable or unstable modal results (poles).

The results obtained from different modal identification methods are shown in Figure 4. As shown, the results from N4SID are closely consistent with either SSI-COV or SSI-DATA. However, there are more modal results in SSI-COV than in SSI-DATA, which may result from differences in the solution method.

As shown in Figure 4, the Complex Mode Indicator Function (CMIF) is used for method verification, which is defined as [41]

$$CMIF_k(j\omega) = \sigma_k^2(j\omega) \tag{15}$$

where $\sigma_k(j\omega)$ is the k -th singular value of the frequency response function (FRF) matrix $H(f)$ at circular frequency $\omega = 2\pi f$, i.e.,

$$H(f) = U(f)S(f)V(f) \tag{16}$$

$$S(f) = \begin{bmatrix} \sigma_1(j\omega) & & & & \\ & \ddots & & & \\ & & \sigma_k(j\omega) & & \\ & & & \ddots & \\ & & & & \sigma_n(j\omega) \end{bmatrix} \tag{17}$$

where $U(f)$ and $V(f)$ are the complex unitary matrices and $S(f)$ is a rectangular diagonal matrix with non-negative real numbers on the diagonal. The diagonal entries of $S(f)$ are uniquely determined by $H(f)$ and are known as the singular values. The maximum of the CMIF corresponds to the characteristic frequency of the system.

As shown in Figure 4, the CMIF maxima are the same in SSI-COV and SSI-DATA results, as the FRF results obtained from the structural monitoring data are identical for the same monopile. Meanwhile, the maxima of the CMIF results coincide with the N4SID results, which is evidence that the modal identification results are convincing. As the three modal identification methods provide satisfactory results here, the N4SID algorithm is used in the rest of the paper, considering its benefits in computation cost and postprocessing of the results.

To eliminate fake modes resulting from mathematical poles and to determine the mode order for modal matching in the inverse evaluation, the modal assurance criterion (MAC), defined as the cross-operation results between all identified mode shape vectors, is used here. The MAC is defined as [42]

$$MAC(\Psi_i, \Psi_j) = \frac{|\Psi_i^* \Psi_j|^2}{\|\Psi_i\|_2^2 \|\Psi_j\|_2^2} \tag{18}$$

where Ψ_i and Ψ_j are the mode shape, with order i and j .

Table 5. Modal results obtained by N4SID (first ten orders). \circ and \times correspond to stable or unstable modal results (poles).

Order	1	2	3	4	5	6	7	8	9	10
Frequency	0.060	0.279	0.420	1.603	1.980	2.020	3.108	3.431	4.029	4.238
Damping ratio	1.000	0.095	0.152	1.000	0.099	0.058	0.469	0.076	0.071	0.447
Type	\times	\circ	\times	\times	\circ	\circ	\times	\circ	\circ	\times

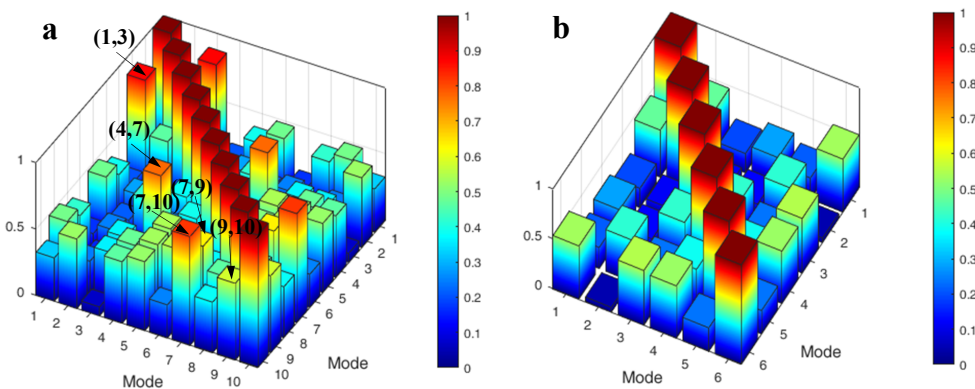


Figure 5. MAC results of first ten identified modal results: (a) original results and (b) with fake modes removed.

The first ten mode results from N4SID are shown in Table 5. The corresponding MAC results are shown in Figure 5. Multiple large non-diagonal values (greater than 0.5) appeared in the MAC results in the modal identification results, indicating the presence of several highly correlated modes. Furthermore, it can be seen from Table 5 that unstable modes with large damping ratios (greater than 10%) appear in the modal results, which are physically unrealizable and can be considered as results from highly correlated mode shapes. Figure 5b shows the results with the fake modes removed. The corresponding MAC results are satisfactory, indicating that the correlation between each mode meets the requirements for stable modal results.

The above discussion confirms that stable modal results can be identified and separated satisfactorily. However, as we need to use the modal results for inverse evaluation, it is necessary to check whether the modal frequencies are invariant or are only engaged with slow or minor changes, i.e., approximately constant, during a relatively long time (for example, one day).

3.1.2. Checking the Stationary Modal Frequencies

According to the modal identification and verification procedures proposed above, the results at different times in a day are shown in Figure 6 (only the results for the first ten orders are included). Time IDs are custom labels used to identify different times in a day, with no practical significance otherwise. In addition, Time IDs 1 to 4 correspond to the initial startup of the studied wind turbine, which is unstable in its working state, while Time IDs 5 to 24 correspond to power production. To eliminate the uncertainty in

the working state of the wind turbine, the following discussion focuses on the results from Time IDs 5 to 24.

As shown in Figure 6, the first-order modal frequencies of the offshore wind turbine during power production are approximately constant, varying between 0.247 Hz and 0.291 Hz, with a median characteristic frequency of 0.274 Hz repeatedly occurring at a different time in one day. However, the corresponding frequencies are slightly changed at other times, with a median fluctuation range of -10% to 5.9% compared to the characteristic frequency. Meanwhile, the damping ratios show an irregular and drastic change between 0 and 10%.

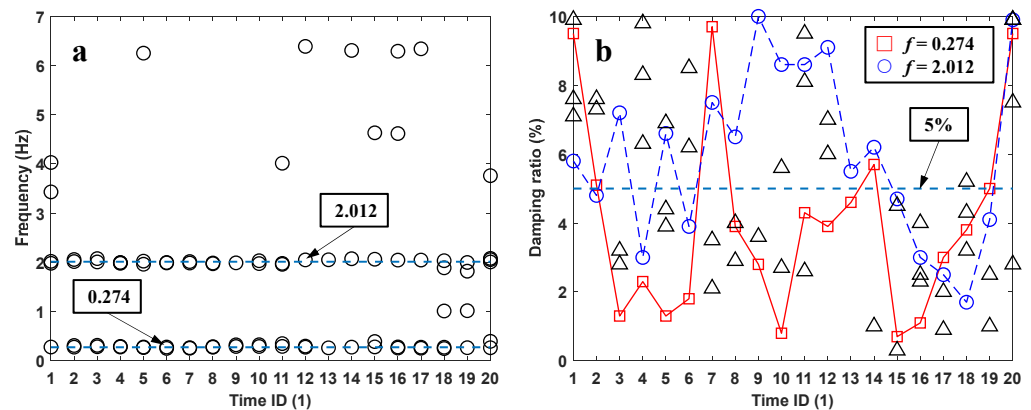


Figure 6. Modal frequencies at different times (Time IDs) in a day: (a) modal frequencies and (b) damping ratios.

The above results quantitatively confirm that the first-order modal frequencies of offshore wind turbines are not a constant value during power production. On the other hand, it confirms that the first-order modal frequencies can be considered approximately constant here, and that a first-order modal frequency $f_0 = 0.274$ Hz can be used.

A further comment should be made here. Based on the above results, it is difficult to determine whether the first-order modal frequencies continue to exist in whole or in part for longer periods, such as 48 h or longer. However, it is sufficient for our purposes here to demonstrate the proposed inverse evaluation method. Further work is needed to reveal the modal characteristics of offshore wind turbines during their working state.

3.2. Verification of Inverse Evaluation Method

3.2.1. Selection of Sensitive Parameters

According to the geotechnical report of the wind farm, the investigated offshore wind turbine is installed on a site with eight marine soil strata. As shown in Table 4, each soil stratum is classified as silt, clay, or sand according to the grain size, with five, three, or seven parameters in each stratum, respectively. The eight soil strata are composed of forty-two parameters categorized into nine types. For the convenience of parameter selection, it is temporarily assumed that the coefficient of variation used to screen the sensitive parameters of the soil layer is $\kappa = 0.5$.

According to the single-factor sensitivity analysis results, the soil parameters can be classified into four categories, i.e., highly sensitive, sensitive, marginally related, and uncorrelated. Selected sensitivity analysis results for the first two categories are shown in Figure 7. The rest of the sensitivity results are omitted, as the idea behind the selection criterion is easy to understand. Meanwhile, as there are deficiencies in the geological measurement mechanisms of certain parameters that may lead to deviations in the geotechnical results, a total of thirty parameters for random search and inversion are considered here based on the sensitivity analysis.

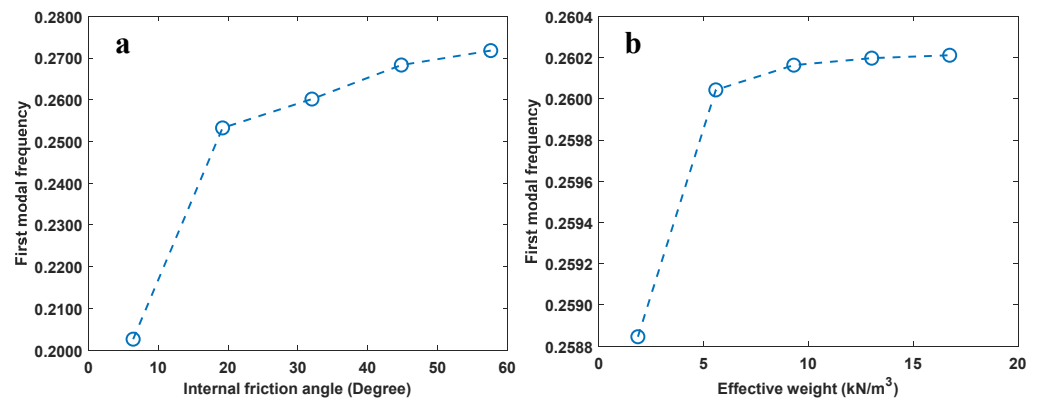


Figure 7. Sensitivity analysis results of selected soil parameters (for illustration only): (a) internal friction angle and (b) effective weight.

3.2.2. Convergence Verification

Iterative optimization can be carried out by selecting all parameters (a total of forty-two) or selected sensitive parameters (a total of thirty). Considering the computing capacity of our workstation (Intel i9 12950HX, NVIDIA RTX A3000, 128 Gigabyte RAM, 2 Terabyte Solid State Disk), the maximum number of iterations was set to $n = 100$ and the convergence criterion was set to a residual of the objective function not greater than 10^{-4} . It was found that the computation time for one parameter case required approximately two to six hours.

During parameter iteration, we found that certain combinations of independent parameters led to cases in which the pile solution (either axial or lateral) failed to converge or in which the combined reduced structural stiffness matrix and pilehead stiffness matrix were non-positive definite. These parameter combinations can lead to physically meaningless or erroneous results. Therefore, these parameter cases were removed, with only the valid iterations plotted versus the objective function’s residual.

The convergence curve of a typical calculation case is shown in Figure 8. As shown, the results confirm that this method can converge to a specific soil parameter combination, which is considered the actual soil parameter during the working state of the wind turbine.

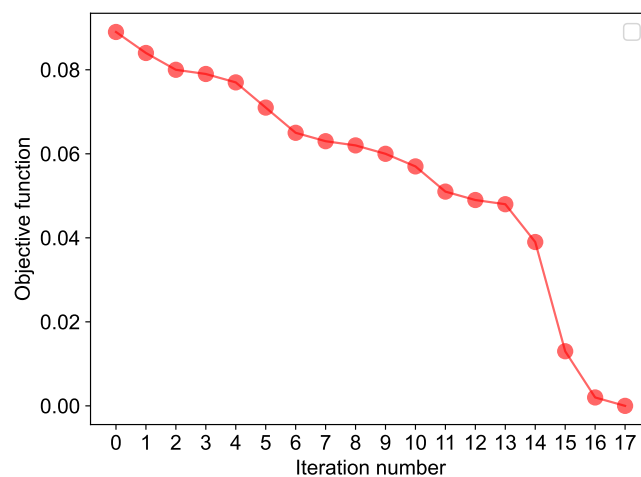


Figure 8. Convergence curve of a typical calculation case.

3.2.3. Sensitivity Analysis of Initial Parameters

Optimization methods can be confusing when they are susceptible to initial values. To check the ability of the algorithm to always converge even under arbitrary parameter cases, five different parameter cases are proposed to show the convergence characteristics. The convergence curves are provided in Figure 9.

As shown in Figure 9, all initial parameter cases (large objective function values corresponding to iteration numbers equaling zero) can converge to desirable objective function values (approximately zero). Meanwhile, although the convergence rate varies with different initial parameter cases, the ideal objective function value (less than 2.0‰) can be reached in four iterations at the least. All initial parameter cases shown can reach the convergence criterion in roughly ten iterations. Therefore, whatever the initial parameter values, the algorithm can always converge after several iterations corresponding to the in situ parameter values.

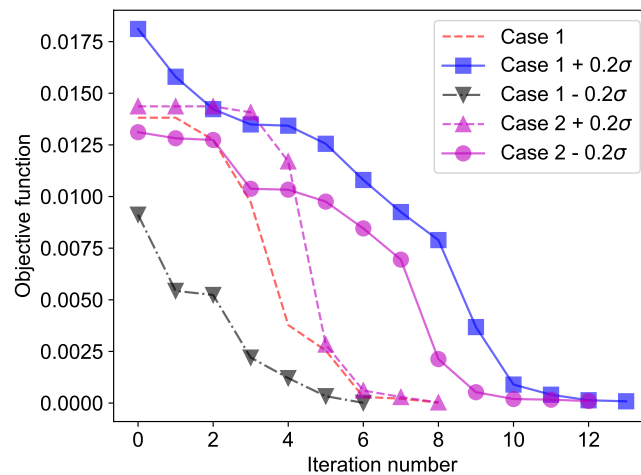


Figure 9. Convergence curves of different initial parameter cases. Cases 1 and 2 correspond to different initial parameter combinations, while σ corresponds to the standard deviation of the parameters.

The initial parameters can be considered as parameters provided for the initial design of offshore wind turbines, which are always obtained by the geotechnical report of the wind farm. As a result of poor geotechnical investigation work, these parameters are sometimes found to deviate considerably from the actual values.

The results in this subsection confirm that whatever the provided parameters are, the proposed algorithm can always converge to a parameter combination after some number of iterations using the proposed inverse evaluation algorithm. The converged results correspond to the numerical results fitting the monitored results best, implying that the obtained parameters can be considered in situ.

Soil is not an ideally continuous medium, as its physical properties are discrete and spatially related. Therefore, the results of a geotechnical survey are reliable only at a certain probability level. However, the results of the geotechnical survey, i.e., the initial value of the inverse evaluation procedure, are vital, as they represent a significant input in foundation design for offshore wind turbines. Thus, it is necessary to evaluate whether all possible initial parameters obtained from a geotechnical survey can lead to identical or similar results.

3.3. Physical Characteristics of Inverse Evaluation Results

According to the inverse evaluation method, different initial parameter cases may converge to slightly different optimal parameters, i.e., multiple parameter combinations that all fit the monitored results well. In reality, only one combination of parameters should exist for the in situ parameters. Therefore, it is necessary to compare the results from different initial parameter cases to determine whether the structural response is numerically similar.

Based on the in situ monitoring data of an offshore wind farm in Jiangsu Province, China, five parameter combinations were obtained using the proposed inverse evaluation method regarding different initial parameter cases. Using these different parameter results from the inverse evaluation method, several design targets regarding monopiles, such as

axial capacities and displacements, were analyzed, and the resulting deviations between the different results were compared. These results can be considered as the influence of initial geological parameters, which can shed light on the impact of uncertainty in geological surveys.

3.3.1. Deviation in Axial Capacities

As the axial bearings of monopile foundations are controlled mainly by compression, their tension capacity is not discussed here. Compression capacities solved by the physical model using different inverse evaluation methods are shown in Table 6, where Max.Error corresponds to the maximum relative error between compression capacities.

Table 6. Comparison of compression capacity under different initial parameter cases (kN).

	Case 1	Case 2	Case 3	Case 4	Case 5	Max. Error
Design Capacity	−30,286.2	−28,012	−32,881.8	−30,557.5	−23,787	−27.66%
Maximum force	−8356	−8356	−8356	−8356	−8356	00.00%
Safety factor	3.624	3.352	3.935	3.657	2.847	38.23%
UC	0.276	0.298	0.254	0.273	0.351	38.23%

The safety factor and UC values are shown in Table 6, and are respectively defined as follows:

$$\alpha = R_d / S_d \tag{19}$$

$$UC = 1 / \alpha \tag{20}$$

where R_d and S_d are the maximum axial force and design capacity. According to NB/T 10105-2018 (Code for Design of Wind Turbine Foundations for Offshore Wind Power Projects) [43] issued by the National Energy Administration of China, the ultimate axial capacity of the structure should satisfy

$$\alpha \geq \gamma_0 \tag{21}$$

where the structural importance coefficient γ_0 is usually taken as 1.1.

Because the maximum axial force on the structure is far less than the design capacity, the safety factor is much larger than the importance coefficient γ_0 ; therefore, the difference in the design capacity resulting from different initial parameter cases does not cause any safety risk. However, an excessive safety factor may lead to redundancy and lack of economy in materials.

As shown in Table 6, the axial capacities are different under different parameter cases, with a maximum difference of about 28%. According to the design report of the offshore wind farm, the compression capacity is 27,887 kN; as the maximum compression force is 8356 kN, the compression capacities in the parameter cases all meet the design requirements. However, the design value of the compression capacity parameter in case 5 is less than the original design capacity.

These results suggest that the design axial capacities of offshore wind turbines are sensitive to geological parameters; thus, a sufficient allowance for bearing capacity should be reserved in the design.

3.3.2. Deviation in Pile Displacements

To ensure the normal operation and power generation of offshore wind turbines, the foundation design should meet the requirements for the safe operation of wind turbines. Displacement at several positions on the turbine foundation solved by the physical model using different inverse evaluation methods is shown in Table 7, where Max.Error corresponds to the maximum relative error between the results obtained by different parameter cases. Figure 10 shows the positions for which displacements are provided.

In Table 7, there are differences in the displacement and rotation angles of the tower bottom, pile head, and pile bottom obtained from the inverse evaluation method under different initial parameter cases. The maximum difference in displacement value at the tower bottom under different cases can reach about 3.42 cm, while the maximum difference in rotation angle is about 0.28 degrees. Moreover, the maximum difference in displacement value at the pile head is approximately 1.80 cm and the maximum difference in rotation angle is about 0.28 degrees. The maximum results at the pile bottom are about 0.68 cm and 0.01 degrees, respectively. Although the absolute value differences at the pile bottom (C) are insignificant, these differences indicate the correlation between the pile bottom response and the soil parameters. The accumulated difference caused by the soil parameters results in a relative difference of over 400% under different initial parameter cases.

Table 7. Comparison of displacement (cm) and rotation angle (degree) under different initial parameter cases.

	Case 1	Case 2	Case 3	Case 4	Case 5	Max. Error
X displacement at A	11.8456	14.3527	10.9306	11.6138	12.2302	31.31%
Z displacement at A	-0.8512	-0.9111	-0.7912	-0.8441	-1.0713	-26.14%
Y rotation angle at A	0.3255	0.3534	0.3080	0.3149	0.3327	14.75%
Z rotation angle at A	0.0026	0.0026	0.0026	0.0026	0.0026	0.00%
X displacement at B	2.6962	4.2020	2.4049	2.8400	2.8201	74.73%
Z displacement at B	-0.8018	-0.8617	-0.7418	-0.7947	-1.0219	-27.40%
Y rotation angle at B	0.1728	0.2008	0.1554	0.1623	0.1801	29.23%
Z rotation angle at B	0.0023	0.0023	0.0023	0.0023	0.0023	0.00%
X displacement at C	0.7350	0.7920	0.6800	0.7290	0.9460	39.12%
Y displacement at C	0.7840	0.4080	0.1390	0.1800	0.8190	489.21%
Z displacement at C	0.7840	0.4080	0.1390	0.1800	0.8190	489.21%
Y rotation angle at C	0.0034	0.0126	0.0103	0.0023	0.0034	450.00%
Z rotation angle at C	0.0034	0.0126	0.0103	0.0023	0.0034	450.00%

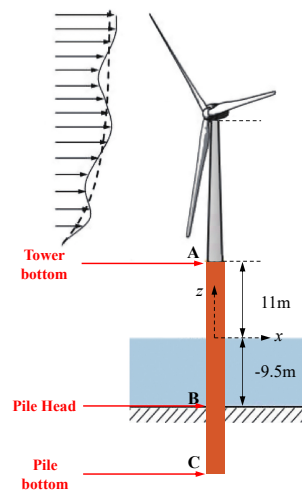


Figure 10. Schematic diagram of positions where displacements on offshore wind turbines were obtained.

According to [43], issued by the National Energy Administration of China, the displacement and rotation at the tower bottom are not specifically controlled, nor are the displacement at the pile head nor the rotation angle at the pile bottom. In accordance with the deformation control requirements for monopile foundations in the NB/T 10105-2018, the displacement at the pile head should be less than 10.8 cm, the rotation angle at the pile head should be less than 0.00436 radians (0.25 degrees), and the displacement at the pile bottom should be less than 10 mm.

According to Table 7, all of the results satisfy the requirements in [43] except for the X displacements at the pile head (position B in Figure 10).

Table 8. Comparison of maximum displacement (cm) and rotation angle (degree) between different initial parameter cases and the design values.

	Case 1	Case 2	Case 3	Case 4	Case 5	Design Values
Displacement at A	11.8456	14.3527	10.9306	11.6138	12.2302	10.36
Rotation at A	0.3255	0.3534	0.3080	0.3149	0.3327	0.2962
Displacement at B	2.6962	4.2020	2.4049	2.8400	2.8201	2.25
Rotation at B	0.1728	0.2008	0.1554	0.1623	0.1801	0.1438
Displacement at C	0.7840	0.7920	0.6800	0.7290	0.9460	0.25

The displacements are further compared with the design results in Table 8. As shown, the maximum displacements and rotation angles are all larger in the inverse evaluation results than those in the design results. These deviations are possible because of soil stiffness distribution deviation resulting from the difference in soil parameters, as the design results are based on the parameters obtained from the geological survey, while the inverse evaluation results are obtained from parameters identified based on monitoring data.

The displacement and rotation angle difference in the two results show that it is possible to underestimate the pile displacement and rotation significantly due to uncertainties in the geological survey.

3.4. Deviation vs. Design Results

To evaluate the current assumptions used in the inverse evaluation procedure, the obtained optimal parameters are introduced to the physical model proposed in Section 2.3.1. The discrepancies in the response of pile foundations between the inverse evaluation results and those of the original design are discussed in this section.

According to the assumptions used during the inverse evaluation, these optimal parameters may correspond to the in situ parameters of offshore wind turbines. Therefore, the discrepancies in the inverse evaluation results and those of the original design can be considered to be issues raised by uncertainty in the design phase of offshore wind turbines. Meanwhile, as these discrepancies resulting from input uncertainty may bring about potentially significant risks, they should be carefully investigated by synthesizing other information on the wind farm.

3.4.1. Discrepancy in Lateral Deflections

The lateral deflections obtained from the inverse evaluation and those of the original design are shown in Figure 11.

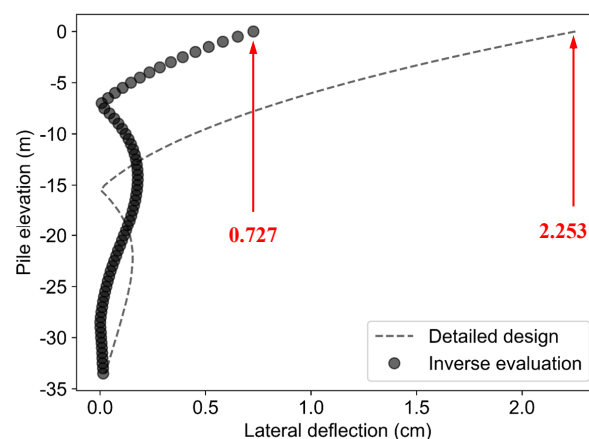


Figure 11. Discrepancy in lateral deflections from different pile evaluations.

As shown in Figure 11, the lateral deflections of the pile foundation at different elevations are roughly different from the original design results; however, although the magnitude of difference may seem significant, the in situ status of the wind turbine is satisfactory, as the lateral deflections are small overall and mostly smaller than the original design, meeting the design requirements of the foundation.

3.4.2. Discrepancy in Axial Deflections

The axial deflections obtained from the inverse evaluation and those of the original design are shown in Figure 12.

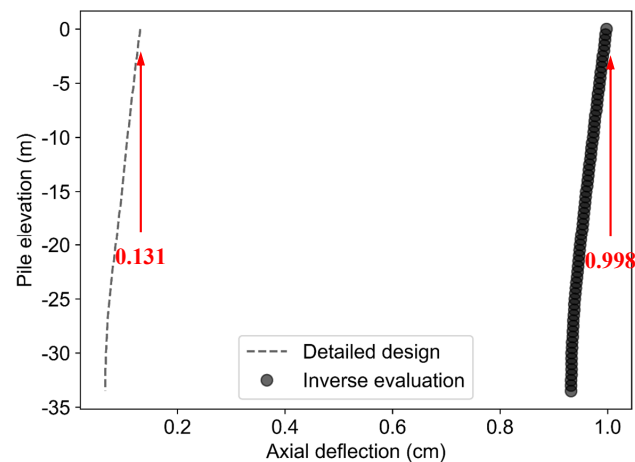


Figure 12. Discrepancy in axial deflections from different pile evaluations.

As shown in Figure 12, the axial deflections of pile foundations at different elevations are significantly different from the original design results. Though the trend is roughly similar, the magnitudes of maximum deflection are 0.131 cm and 0.998 cm, respectively, in the original design and in situ results. This discrepancy in axial deflection results from the difference in soil parameters. The variation in soil parameters can lead to different axial capacities. In this case, the compression capacity obtained from the inverse evaluation is 24,016.8 kN, which is far below the design result (27,887 kN). As a result, the axial deflection is increased compared to the original design. According to [43], the in situ status of the wind turbine is compliant with the standard, as the total deflection at the pile head (pile elevation equal to 0) is less than 10.8 cm.

However, as significant discrepancies in axial deflections are revealed, attention should be paid to the in situ axial capacity and deflection of the offshore wind turbines in this wind farm. The difference indicates that the uncertainty in soil parameters can lead to significantly more considerable in situ axial deflections than the original design results. Therefore, although the current axial deflections are acceptable, the discrepancy between the two results, i.e., the in situ axial deflection and the original design result, implies that attention is required concerning the sensitivity of axial deflection to the soil parameters to avoid potential risks.

3.4.3. Discrepancy in Pile Rotation

The rotations obtained from the inverse evaluation and original design are shown in Figure 13.

As shown in Figure 13, the pile rotations at different elevations are different, though smaller than the original design results, with a maximum value of 0.00153 radians vs. 0.00251 radians. These results are all acceptable according to [43], as all the rotation angles at the pile head (pile elevation equals 0) are less than 0.00436 radians (0.25 degrees). However, it is notable that, with a 39.04% smaller in-situ pile rotation angle, the difference

between the two results is quite significant. This means the original design can be optimized for the pile rotation should it be the design constraint.

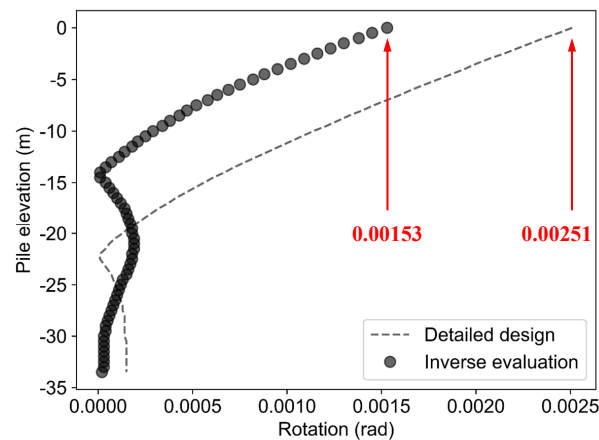


Figure 13. Discrepancy in pile rotation from different pile evaluations.

3.5. Limitations of the Proposed Inverse Evaluation Method

Based on the measured results and the numerical model, we proposed a parameter inversion method for the pile–soil interaction model using soil reaction curves. This method is promising and straightforward to implement; however, there are several flaws that should be noted.

First, the obtained results are related to the selected numerical model. Therefore, the proposed method can only correct the relevant parameters of the numerical model, and cannot overcome the shortcomings of the numerical model itself. A more realistic numerical model would make for more realistic results.

Second, the parameter space is based on certain assumptions. However, the actual distribution of the model parameters is uncertain. A more realistic parameter distribution would mean a faster search for actual results, if any.

Finally, the calculation efficiency needs to be further improved. Surrogate models, such as the response surface models, could be considered in subsequent research to accelerate calculation under the premise of maintained reliability.

4. Conclusions

Using monitoring data from an offshore wind farm in the East China Sea and numerical models, we proposed a parameter inversion method for a pile–soil interaction model based on the measured results and the numerical model. The proposed parameter inversion method involves several steps. First, it is necessary to construct a numerical model. Then, after the in situ modal frequencies have been identified as stable, an objective function can be selected using both the numerical and identified results. Subsequently, inverse optimization is performed using a random search algorithm in the assumed parameter space. The parameter results in the minimum optimization objective function are identified as the in situ parameters of the monopile, which result in the numerical model that best approximates the in situ structure. Our convergence verification results confirmed that this method could converge to a specific soil parameter combination. Furthermore, our results showed that whatever the initial parameter values, the proposed method can always converge after some number of iterations corresponding to the in situ parameter values. However, it was found that different initial parameter cases may converge to slightly different optimal parameters, i.e., deviations in axial capacities or pile displacements, implying that the pile results are sensitive to geological parameters. Therefore, it is necessary to make a sufficient allowance for uncertainties in geological surveys. The results obtained by the proposed method were compared with the original design results to check for design

redundancy or risks. Although the proposed method has several flaws, it can shed light on the influence of parameter uncertainties on offshore wind turbines.

Author Contributions: Conceptualization, H.Q., W.L. and C.G.; methodology, H.Q. and C.G.; software and validation, H.Q. and C.G.; formal analysis and investigation, W.L. and X.S.; resources, Z.J. and X.S.; data curation, H.Q.; writing—original draft preparation, H.Q. and W.L.; writing—review and editing, Z.J., X.S. and C.G.; visualization, H.Q.; supervision, Z.J., X.S. and C.G.; project administration, W.L. and Z.J.; funding acquisition, W.L. and Z.J. All authors have read and agreed to the published version of the manuscript.

Funding: This work was supported by the Guangdong Provincial Science and Technology Plan Project (No. 2019B111106002), National Key Research and Development Program of China (No. 2021YFF0502200), National Natural Science Foundation of China (No. 52008264), Shenzhen Science and Technology Program (No. JCYJ20220818100202006, No.20220810160740001), Hong Kong Research Grants Council (No. PolyU 152634/16E and T22-502/18-R), and Hong Kong Polytechnic University (No. 1-BBAG).

Institutional Review Board Statement: Not applicable.

Informed Consent Statement: Not applicable.

Data Availability Statement: Data are available on request.

Conflicts of Interest: The authors declare no conflict of interest. The funders had no role in the design of the study, in the collection, analysis, or interpretation of the data, in the writing of the manuscript, or in the decision to publish the results.

References

- Jahani, K.; Langlois, R.G.; Afagh, F.F. Structural dynamics of offshore Wind Turbines: A review. *Ocean. Eng.* **2022**, *251*, 111136. [[CrossRef](#)]
- Devriendt, C.; Weijtjens, W.; El-Kafafy, M.; De Sitter, G. Monitoring resonant frequencies and damping values of an offshore wind turbine in parked conditions. *IET Renew. Power Gener.* **2014**, *8*, 433–441. [[CrossRef](#)]
- Häckell, M.W.; Rolfes, R. Monitoring a 5 MW offshore wind energy converter—Condition parameters and triangulation based extraction of modal parameters. *Mech. Syst. Signal Process.* **2013**, *40*, 322–343. [[CrossRef](#)]
- Devriendt, C.; Magalhães, F.; Weijtjens, W.; De Sitter, G.; Cunha, Á.; Guillaume, P. Structural health monitoring of offshore wind turbines using automated operational modal analysis. *Struct. Health Monit.* **2014**, *13*, 644–659. [[CrossRef](#)]
- Xu, M.; Au, F.T.; Wang, S.; Wang, Z.; Peng, Q.; Tian, H. Dynamic response analysis of a real-world operating offshore wind turbine under earthquake excitations. *Ocean. Eng.* **2022**, *266*, 112791. [[CrossRef](#)]
- Koukoura, C.; Natarajan, A.; Vesth, A. Identification of support structure damping of a full scale offshore wind turbine in normal operation. *Renew. Energy* **2015**, *81*, 882–895. [[CrossRef](#)]
- Chen, B.; Zhang, Z.; Hua, X.; Basu, B.; Nielsen, S.R. Identification of aerodynamic damping in wind turbines using time-frequency analysis. *Mech. Syst. Signal Process.* **2017**, *91*, 198–214. [[CrossRef](#)]
- Bajrić, A.; Høgsberg, J.; Rüdinger, F. Evaluation of damping estimates by automated operational modal analysis for offshore wind turbine tower vibrations. *Renew. Energy* **2018**, *116*, 153–163. [[CrossRef](#)]
- Van Vondelen, A.A.; Navalkar, S.T.; Iliopoulos, A.; van der Hoek, D.C.; van Wingerden, J.W. Damping identification of offshore wind turbines using operational modal analysis: A review. *Wind. Energy Sci.* **2022**, *7*, 161–184. [[CrossRef](#)]
- Dong, X.; Lian, J.; Wang, H.; Yu, T.; Zhao, Y. Structural vibration monitoring and operational modal analysis of offshore wind turbine structure. *Ocean. Eng.* **2018**, *150*, 280–297. [[CrossRef](#)]
- Oliveira, G.; Magalhães, F.; Cunha, Á.; Caetano, E. Vibration-based damage detection in a wind turbine using 1 year of data. *Struct. Control. Health Monit.* **2018**, *25*, e2238. [[CrossRef](#)]
- Dong, X.; Lian, J.; Yang, M.; Wang, H. Operational modal identification of offshore wind turbine structure based on modified stochastic subspace identification method considering harmonic interference. *J. Renew. Sustain. Energy* **2014**, *6*, 033128. [[CrossRef](#)]
- Liu, F.; Gao, S.; Tian, Z.; Liu, D. A new time-frequency analysis method based on single mode function decomposition for offshore wind turbines. *Mar. Struct.* **2020**, *72*, 102782. [[CrossRef](#)]
- Liu, F.; Gao, S.; Han, H.; Tian, Z.; Liu, P. Interference reduction of high-energy noise for modal parameter identification of offshore wind turbines based on iterative signal extraction. *Ocean. Eng.* **2019**, *183*, 372–383. [[CrossRef](#)]
- Martinez-Luengo, M.; Shafiee, M.; Kolios, A. Data management for structural integrity assessment of offshore wind turbine support structures: Data cleansing and missing data imputation. *Ocean. Eng.* **2019**, *173*, 867–883. [[CrossRef](#)]
- Qiu, Y.; Feng, Y.; Infield, D. Fault diagnosis of wind turbine with SCADA alarms based multidimensional information processing method. *Renew. Energy* **2020**, *145*, 1923–1931. [[CrossRef](#)]

17. Iliopoulos, A.; Shirzadeh, R.; Weijtjens, W.; Guillaume, P.; Van Hemelrijck, D.; Devriendt, C. A modal decomposition and expansion approach for prediction of dynamic responses on a monopile offshore wind turbine using a limited number of vibration sensors. *Mech. Syst. Signal Process.* **2016**, *68*, 84–104. [[CrossRef](#)]
18. Maes, K.; Iliopoulos, A.; Weijtjens, W.; Devriendt, C.; Lombaert, G. Dynamic strain estimation for fatigue assessment of an offshore monopile wind turbine using filtering and modal expansion algorithms. *Mech. Syst. Signal Process.* **2016**, *76*, 592–611. [[CrossRef](#)]
19. Nabiyani, M.S.; Khoshnoudian, F.; Moaveni, B.; Ebrahimian, H. Mechanics-based model updating for identification and virtual sensing of an offshore wind turbine using sparse measurements. *Struct. Control. Health Monit.* **2021**, *28*, e2647. [[CrossRef](#)]
20. Bisoi, S.; Haldar, S. Design of monopile supported offshore wind turbine in clay considering dynamic soil-structure-interaction. *Soil Dyn. Earthq. Eng.* **2015**, *73*, 103–117. [[CrossRef](#)]
21. Andersen, L.V.; Vahdatirad, M.J.; Sichani, M.T.; Sørensen, J.D. Natural frequencies of wind turbines on monopile foundations in clayey soils—A probabilistic approach. *Comput. Geotech.* **2012**, *43*, 1–11. [[CrossRef](#)]
22. Negro, V.; López-Gutiérrez, J.S.; Esteban, M.D.; Matutano, C. Uncertainties in the design of support structures and foundations for offshore wind turbines. *Renew. Energy* **2014**, *63*, 125–132. [[CrossRef](#)]
23. Clouteau, D.; Cottureau, R.; Lombaert, G. Dynamics of structures coupled with elastic media—A review of numerical models and methods. *J. Sound Vib.* **2013**, *332*, 2415–2436. [[CrossRef](#)]
24. Kausel, E. Early history of soil-structure interaction. *Soil Dyn. Earthq. Eng.* **2010**, *30*, 822–832. [[CrossRef](#)]
25. Damgaard, M.; Zania, V.; Andersen, L.V.; Ibsen, L.B. Effects of soil-structure interaction on real time dynamic response of offshore wind turbines on monopiles. *Eng. Struct.* **2014**, *75*, 388–401. [[CrossRef](#)]
26. Arany, L.; Bhattacharya, S.; Adhikari, S.; Hogan, S.; Macdonald, J.H.G. An analytical model to predict the natural frequency of offshore wind turbines on three-spring flexible foundations using two different beam models. *Soil Dyn. Earthq. Eng.* **2015**, *74*, 40–45. [[CrossRef](#)]
27. Zania, V. Natural vibration frequency and damping of slender structures founded on monopiles. *Soil Dyn. Earthq. Eng.* **2014**, *59*, 8–20. [[CrossRef](#)]
28. Peeters, B.; Roeck, G.D. Reference-based stochastic subspace identification for output-only modal analysis. *Mech. Syst. Signal Process.* **1999**, *13*, 855–878. [[CrossRef](#)]
29. Reynders, E. System identification methods for operational modal analysis: Review and comparison. *Arch. Comput. Methods Eng.* **2012**, *19*, 51–124. [[CrossRef](#)]
30. Overschee, P.; Moor, B. *Subspace Identification for Linear Systems: Theory—Implementation—Applications*; Springer Science & Business Media: Berlin/Heidelberg, Germany, 2012.
31. Van Overschee, P.; De Moor, B. N4SID: Subspace algorithms for the identification of combined deterministic-stochastic systems. *Automatica* **1994**, *30*, 75–93. [[CrossRef](#)]
32. Verhaegen, M. Identification of the deterministic part of MIMO state space models given in innovations form from input-output data. *Automatica* **1994**, *30*, 61–74. [[CrossRef](#)]
33. *Wind energy generation systems: Part 3-1: Design requirements for fixed offshore wind turbines (IEC 61400-3-1:2019)*; The British Standards Institution: London, UK, 2019.
34. Santra, P.; Chopra, U.; Chakraborty, D. Spatial variability of soil properties and its application in predicting surface map of hydraulic parameters in an agricultural farm. *Curr. Sci.* **2008**, 937–945.
35. Gupta, R.K.; Abrol, I.P.; Finkl, C.W.; Kirkham, M.B.; Arbustain, M.C.; Macías, F.; Chesworth, W.; Germida, J.J.; Loeppert, R.H.; Cook, M.G.; et al. Soil Variation. In *Encyclopedia of Soil Science*; Chesworth, W., Ed.; Springer: Dordrecht, The Netherlands, 2008; pp. 705–707.
36. Young, R. *Soil Properties and Behaviour*; Elsevier: Amsterdam, The Netherlands, 2012; Volume 5.
37. *Geotechnical and Foundation Design Considerations. ANSI/API Recommended Practice 2GEO, First Edition, April 2011, Addendum 1, October 2014*; American Petroleum Institute: Washington, DC, USA, 2014.
38. Burd, H.J.; Beuckelaers, W.J.A.P.; Byrne, B.W.; Gavin, K.G.; Houlsby, G.T.; Igoe, D.J.P.; Jardine, R.J.; Martin, C.M.; McAdam, R.A.; Wood, A.M.; et al. New data analysis methods for instrumented medium-scale monopile field tests. *Géotechnique* **2020**, *70*, 961–969. [[CrossRef](#)]
39. *DNV-ST-0126 Edition December 2021: Support Structures for Wind Turbines*; DNV AS: Oslo, Norway, 2021.
40. Bergstra, J.; Bengio, Y. Random search for hyper-parameter optimization. *J. Mach. Learn. Res.* **2012**, *13*, 281–305.
41. Peeters, B.; De Roeck, G. Stochastic system identification for operational modal analysis: A review. *J. Dyn. Syst. Meas. Control.* **2001**, *123*, 659–667.
42. Alvin, K.; Robertson, A.; Reich, G.; Park, K. Structural system identification: From reality to models. *Comput. Struct.* **2003**, *81*, 1149–1176.
43. *NB/T 10105-2018 Code for Design of Wind Turbine Foundations for Offshore Wind Power Projects*; National Energy Administration of China: Beijing, China, 2019.

Disclaimer/Publisher’s Note: The statements, opinions and data contained in all publications are solely those of the individual author(s) and contributor(s) and not of MDPI and/or the editor(s). MDPI and/or the editor(s) disclaim responsibility for any injury to people or property resulting from any ideas, methods, instructions or products referred to in the content.